

Finite-frequency prethermalization in periodically driven ergodic systems

Lorenzo Correale,^{1,2} Leticia F. Cugliandolo,^{3,4} Marco Schirò,⁵ and Alessandro Silva¹

¹SISSA — International School for Advanced Studies, via Bonomea 265, I-34136 Trieste, Italy

²INFN — Istituto Nazionale di Fisica Nucleare, Sezione di Trieste, I-34136 Trieste, Italy

³Sorbonne Université, Laboratoire de Physique Théorique et Hautes Energies,
CNRS UMR 7589, 4 Place Jussieu, 75252 Paris Cedex 05, France

⁴Institut Universitaire de France, 1 rue Descartes, 75005 Paris France

⁵JEIP, UAR 3573 CNRS, Collège de France, PSL Research University,
11 Place Marcelin Berthelot, 75321 Paris Cedex 05, France

(Dated: January 9, 2024)

We investigate the periodically driven dynamics of many-body systems, either classical or quantum, finite-dimensional or mean-field, displaying an unbounded phase-space. We find that the inclusion of a smooth periodic drive atop an otherwise ergodic dynamics leads to a long-lived prethermalization, even at moderate driving frequencies. In specific asymptotic limits, we compute the corresponding prethermal Hamiltonian from an analytical perturbation scheme.

Introduction — Periodically-driven systems are known to host a great deal of non-trivial phenomena. For example, an inverted pendulum can be stabilized by an external force oscillating at sufficiently high frequency [1], while a kicked-rotor exhibits an integrability-to-chaos transition [2] that is counter-intuitively suppressed by the inclusion of quantum fluctuations [3]. Similarly, a driven quantum single particle system may localize in energy space resulting in bounded heating [4]. While single-particle systems have been the focus of research in the past decades, attention has recently shifted towards many-particle ones, which have proven to be valuable tools to reproduce experimentally a wide array of novel phases of matter, within the field of *Floquet engineering* [5]. However, a major obstacle to their practical realization has been the fact that periodically driven isolated many-body systems tend to quickly heat up to a featureless infinite-temperature state, due to the absence of conservation laws [6–9].

Infinite-temperature thermalization can be avoided by many-body localization [10–12] and integrability [13–19]. For generic short-range interacting systems, heating can be suppressed only in a finite time window. For example, a prethermalization induced by a high-frequency drive Ω has been observed in numerical studies both in classical [20–22] and quantum systems [23–30], as well as in some experimental setups [31–34]. In this case, the corresponding prethermal Hamiltonian is asymptotically close to the average over a period, $\overline{H(t)}$, of the true periodic Hamiltonian $H(t)$. While most literature has concentrated on systems with a locally bounded energy spectrum, high-frequency prethermalization has been conjectured as a generic outcome also for unbounded spectra [35], as supported by numerical studies on periodically kicked systems [22, 36, 37] and experiments involving a uniform Fermi gas [34].

From a broader perspective, prethermalisation is also observed close to an integrable point, both in quenched systems [38] as well as under periodic drive [39]. Beyond

these scenarios, the conventional expectation is that a non-integrable system with intermediate-coupling interactions and drive frequency should rapidly thermalize. In this work, we show that this expectation is not met when a system with an unbounded energy spectrum is driven under a smooth periodic force.

We investigate two systems, namely the 1D lattice ϕ^4 model and the p -spin spherical model (PSM). For the parameters we choose, the dynamics of both models rapidly relax to thermal equilibrium in absence of the drive. Instead, the coupling to an external drive leads the systems to prethermalize with an effective Hamiltonian \mathcal{H}_F which is not just a time-average of the unperturbed one. For the ϕ^4 model, we calculate \mathcal{H}_F in certain asymptotic, but not necessarily high-frequency, limits. Additionally, in both classical and quantum PSMs, an approximate classical fluctuation-dissipation relation supports the likelihood of approaching a prethermal finite-temperature state.

The classical 1D lattice ϕ^4 model — The model is

$$H_{\phi^4}(\mathbf{x}, \mathbf{p}) = \sum_{i=1}^N \left[\frac{p_i^2}{2} + \frac{\omega_0^2}{2} x_i^2 + \frac{\lambda}{4} x_i^4 + \frac{g}{2} (x_{i+1} - x_i)^2 \right] \quad (1)$$

with $\omega_0^2 > 0$ and periodic boundary conditions. The normal modes of its quadratic part have frequencies $\omega_k = \sqrt{\omega_0^2 + 2g[1 - \cos(2\pi k/N)]}$, for $k = 0 \dots N - 1$. In absence of an external drive and for the parameters we consider here, the Hamilton dynamics displays ergodicity [40, 41] (see also the SM [42]) and chaos [43, 44]. Several experimental realizations have been proposed for its quantum extension [45–47]. We aim to study the dynamics driven by the term $H_1(\mathbf{x}, t) = -B_0 \sin(\Omega t) \sum_i x_i$. The classical equations of motion are

$$\ddot{x}_i + \omega_0^2 x_i = B_0 \sin(\Omega t) + g(x_{i+1} - 2x_i + x_{i-1}) - \lambda x_i^3, \quad (2)$$

for $i = 1, \dots, N$. In Fig. 1 we plot the energy density, $e(t) = \langle H_{\phi^4}(\mathbf{x}(t), \dot{\mathbf{x}}(t)) \rangle_0 / N$, averaged over \mathcal{N} initial conditions randomly sampled on $H_{\phi^4}(\mathbf{x}(0), \dot{\mathbf{x}}(0)) = Ne_0$, a constant energy manifold. For all values of e_0 (a) and Ω

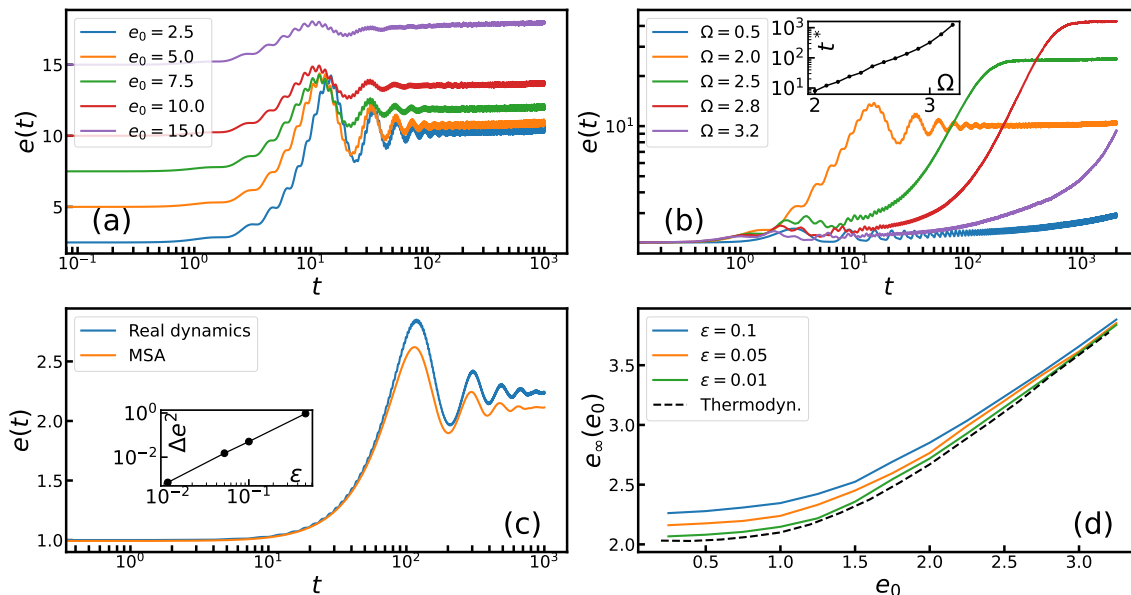


FIG. 1. One dimensional lattice ϕ^4 model with $N = 100$. Data averaged over $\mathcal{N} = 1000$ configurations. (a)-(b) The energy density $e(t) = \langle H_{\phi^4}(\mathbf{x}(0), \dot{\mathbf{x}}(0)) \rangle_{H_0} / N$, obtained by integrating Eqs. (2), with $B_0 = g = \lambda = \omega_0^2 = 1$. (a) $\Omega = 2.4$ and several e_0 . (b) $e_0 = 2$ and several Ω . Inset: time t^* where $e(t)$ crosses the threshold $e_1 = 8$ for the first time, for several Ω . (c) Comparison between $e(t)$ and the energy density in Eq. (8) estimated from the effective dynamics in Eqs. (7), with $e_0 = \Omega = \tilde{B}_0 = \tilde{g} = \tilde{\lambda} = 1$, $\Delta\omega^2 = 3$, $\epsilon = 0.05$. The parameters of Eq. (2) are determined by the rescaling in the main text. Inset: time-averaged difference Δe^2 , between the real and the MSA dynamics, as defined in Eq. (9). To avoid transient effects, we perform the time-average over a window $[3/4 t_{max}, t_{max}]$, with t_{max} the maximum simulation time. (d) e_0 dependence of the asymptotic energy density e_∞ , computed as the average Eq. (12) over the same late time window of the dynamics in Eqs. (2). The dependence on ϵ is introduced through $\tilde{B}_0, \tilde{g}, \tilde{\lambda}$. The dashed line is a microcanonical average, Eqs. (11) and (10).

(b), $e(t)$ saturates to a finite e_∞ at long times, signalling prethermalization. This result remains robust even when choosing a different $H_1(\mathbf{x}, t)$ [42]. By integrating the dynamics over a longer time scale and for several values of λ , we observe deviations of $e(t)$ from e_∞ which suggest a finite life-time of the plateau controlled by λ [42]. When Ω is roughly outside the spectrum of normal mode frequencies of Eq. (1), the growth of $e(t)$ slows down. For large Ω , we quantitatively estimate the slowdown from the time t^* at which $e(t)$ crosses a threshold $e_1 \in [0, e_\infty]$. The inset of Fig. 1(b) illustrates that $t^* \sim \exp(c\Omega)$ for sufficiently large Ω . This dependence resembles the one of the high-frequency prethermalization time in classical and quantum spin chains [20, 29].

The crucial observation that we make is that e_∞ typically differs from the initial energy e_0 . This result suggests that, assuming the prethermal state to be Gibbs-like, the corresponding effective Hamiltonian should be distinct from $H_{\phi^4}(\mathbf{x}, \mathbf{p})$. To gain some analytical insight on this phenomenon, we study the limit of small driving amplitude and interaction, by rescaling the parameters as $B_0 = \epsilon \tilde{B}_0$, $\lambda = \epsilon \tilde{\lambda}$ and $g = \epsilon \tilde{g}$, for $\epsilon \ll 1$. We also rescale the driving frequency to $\omega_0 = \sqrt{\Omega^2 - \epsilon \Delta\omega^2}$, keeping $\Omega \sim O(1)$, to enable energy absorption through parametric resonances [48] even when Eqs. (2) are close to the ones of non-interacting harmonic oscillators at fre-

quency ω_0 [49]. Standard perturbative methods fail even at small ϵ , due to the proliferation of secular terms. We circumvent this problem by employing a multiple-scale analysis (MSA) [50], a method already used to study single-particle Floquet systems in their high-frequency limit [51]. Here we briefly review the method, details are postponed to the Supplemental Material (SM) [42]. We begin by introducing a redundant variable $\tau = \epsilon t$, representing the ‘slow’ time-scale over which the growth of $e(t)$ is expected. We propose the asymptotic expansion

$$x_i(t) = x_{0,i}(t, \tau) + \epsilon x_{1,i}(t, \tau) + \dots \quad (3)$$

and treat t and τ as they were *independent*. Although the exact solution $\mathbf{x}(t)$ depends only on t , this trick is useful to eliminate secular terms at each perturbative order. We plug Eq. (3), together with the chain rule $d/dt = \partial_t + \epsilon \partial_\tau$, into Eq. (2). After collecting powers of ϵ , the first two perturbative orders read:

$$(\partial_t^2 + \Omega^2) x_{0,i} = 0, \quad (4)$$

$$(\partial_t^2 + \Omega^2) x_{1,i} = -2\partial_t \partial_\tau x_{0,i} + \Delta\omega^2 x_{0,i} - \tilde{\lambda} x_{0,i}^3 + \tilde{B}_0 \sin(\Omega t). \quad (5)$$

The solution of Eq. (4) is given by

$$x_{0,i}(t, \tau) = u_i(\tau) \cos(\Omega t) + v_i(\tau) \sin(\Omega t). \quad (6)$$

The slowly varying amplitudes $u_i(\tau)$ and $v_i(\tau)$ are determined by imposing that secular terms, proportional to $\sin(\Omega t)$ or $\cos(\Omega t)$, are absent in the right-hand-side of Eq. (5), the next order, as these would predict a divergence which we do not observe numerically. After some algebra [42], one finds the Hamiltonian equations

$$\frac{du_i}{d\tau} = -\frac{\partial \mathcal{H}_F}{\partial v_i}, \quad \frac{dv_i}{d\tau} = \frac{\partial \mathcal{H}_F}{\partial u_i}, \quad (7)$$

generated by the many-body, local effective Hamiltonian

$$\mathcal{H}_F(\mathbf{u}, \mathbf{v}) = \frac{1}{2\Omega} \sum_i \left\{ -\frac{\Delta\omega^2}{2}(u_i^2 + v_i^2) + \frac{\tilde{g}}{2}[(u_{i+1} - u_i)^2 + (v_{i+1} - v_i)^2] + \frac{3\tilde{\lambda}}{16}(u_i^2 + v_i^2)^2 + \tilde{B}_0 v_i \right\}.$$

Plugging the leading order $x_{0,i}(t, \tau)$ into Eq. (1), the estimate of the energy density is

$$\begin{aligned} e^{\text{MSA}}(t) &= \frac{1}{N} \langle H_{\phi^4}[\mathbf{x}_0(t, \tau), \partial_t \mathbf{x}_0(t, \tau)] \rangle_0 \Big|_{\tau=\epsilon t} = \\ &= \frac{1}{N} \langle \mathcal{H}_0[\mathbf{u}(\tau), \mathbf{v}(\tau)] \rangle_0 \Big|_{\tau=\epsilon t} + O(\epsilon). \end{aligned} \quad (8)$$

The Hamiltonian $\mathcal{H}_0(\mathbf{u}, \mathbf{v}) = \Omega^2 \sum_i (u_i^2 + v_i^2)/2$ is obtained omitting the order ϵ terms in g and λ from Eq. (1). The average of $\mathcal{H}_0(\mathbf{u}, \mathbf{v})$ is still performed over microcanonically sampled initial conditions $\mathbf{x}(0)$ and $\dot{\mathbf{x}}(0)$, corresponding to $\mathbf{u}(0) = \mathbf{x}(0)$ and $\mathbf{v}(0) = \dot{\mathbf{x}}(0)/\Omega$ from Eq. (6). In Fig. 1(c), we compare the estimate from Eq. (8) with the results from the full dynamics in Eqs. (2). The MSA successfully reproduces the dynamics up to a finite time as well as the saturation to a finite plateau at e_∞ . Its validity is further confirmed by an investigation of the time-averaged difference

$$\Delta e^2 = \lim_{\mathcal{T} \rightarrow \infty} \frac{1}{\mathcal{T}} \int_0^{\mathcal{T}} dt |e(t) - e^{\text{MSA}}(t)|^2, \quad (9)$$

between $e(t)$ from the dynamics in Eq. (2), and $e^{\text{MSA}}(t)$ from Eq. (8). In particular, we observe that Δe^2 vanishes for vanishing ϵ . Our results suggest that the prethermal state that we observe is indeed generated by an effective Hamiltonian, computed from Eq. (8) at the leading order, which differs from $H_{\phi^4}(\mathbf{x}, \mathbf{p})$ [52] even for a small ϵ .

The primary advantage of the MSA is that it quantitatively predicts the value of e_∞ , for small ϵ , from equilibrium statistical mechanics. We first observe that, as $\mathcal{H}_F(\mathbf{u}, \mathbf{v})$ is conserved by the dynamics in Eqs. (7), the estimate $e^{\text{MSA}}(t)$ in Eq. (8) is expected to relax to the average

$$e_\infty^{\text{MSA}}(e_F) = \langle \mathcal{H}_0(\mathbf{u}, \mathbf{v}) \rangle_F / N, \quad (10)$$

over an *effective* microcanonical ensemble determined by $\mathcal{H}_F(\mathbf{u}, \mathbf{v}) = Ne_F$. The energy density e_F is in turn determined by the average

$$e_F(e_0) = \langle \mathcal{H}_F(\mathbf{u}, \mathbf{v}) \rangle_0 / N, \quad (11)$$

computed over a uniform distribution on the surface $Ne_0 = \mathcal{H}_0(\mathbf{u}, \mathbf{v})$, which approximates the original initial conditions of our protocol, at leading order in ϵ . Combining Eqs. (10) and (11) we obtain the relationship $e_\infty^{\text{MSA}}(e_0)$. To validate this relation, we compare it to $e_\infty(e_0)$ obtained from the dynamics in Eq. (2), averaged over a late time window

$$e_\infty(e_0) = \lim_{\mathcal{T} \rightarrow \infty} \frac{1}{N\mathcal{T}} \int_0^{\mathcal{T}} dt \langle H_{\phi^4}(\mathbf{x}(t), \mathbf{p}(t)) \rangle_0, \quad (12)$$

and initial conditions on the manifold $H_{\phi^4}(\mathbf{x}, \mathbf{p}) = Ne_0$. The comparison, illustrated in Fig. 1(d), demonstrates that the two relations merge for $\epsilon \rightarrow 0$. Our analysis may be improved by including higher-order terms from Eq. (3).

The classical and quantum fully-connected PSM — We can now generalize our findings to classical and quantum systems of mean-field kind, focusing on the driven p -spin spherical model (PSM):

$$\hat{H}_J = \sum_i \frac{\hat{\Pi}_i^2}{2M} - \sum_{i_1 < \dots < i_p} J_{i_1 \dots i_p} \hat{\sigma}_{i_1} \dots \hat{\sigma}_{i_p} - B_0 \sin(\Omega t) \sum_i \hat{\sigma}_i \quad (13)$$

The PSM describes a gas of N particles interacting through random, all-to-all couplings J_{i_1, \dots, i_p} , independently sampled from a Gaussian distribution with zero mean and variance $\overline{J^2} = p! J^2 / 2N^{p-1}$. The particles are globally constrained over an N -sphere, $\sum_i \langle \hat{\sigma}_i^2 \rangle = N$ [53]. Quantum fluctuations are implemented by the canonical quantization relations $[\hat{\sigma}_i, \hat{\Pi}_j] = i\hbar \delta_{ij}$ and are controlled by the dimensionless parameter $\Gamma = \sqrt{\hbar^2/M}$ [54]. In the following, we will set $M = J = 1$. On a critical line $T_c(\Gamma)$, the PSM displays a thermodynamic phase transition between a paramagnetic and a glassy state, which is either of the first or second order depending on the strength of Γ [54, 55]. From a dynamical point of view, the model is ergodic at high-temperatures and non-ergodic below a temperature $T_d(\Gamma) > T_c(\Gamma)$ [56]. Evidences for dynamical and quantum chaos are retrieved in the ergodic and non-ergodic phases [57–60].

We work at $T > T_d(\Gamma)$, where the PSM is ergodic. The symmetric correlation and linear response function

$$C(t, t') = \frac{1}{2} \langle \hat{\sigma}(t) \hat{\sigma}(t') + \hat{\sigma}(t') \hat{\sigma}(t) \rangle, \quad (14)$$

$$R(t, t') = \frac{i}{\hbar} \theta(t - t') \langle [\hat{\sigma}(t), \hat{\sigma}(t')] \rangle, \quad (15)$$

obey a closed set of Schwinger-Dyson equations, valid for $N \rightarrow \infty$ and under disorder average [56, 61–63] (see the SM [42]). We initialize the dynamics by evolving the undriven ($B_0 = 0$) system in contact with a bath of harmonic oscillators at temperature $T_0 > T_d$ during a finite time $0 < t < t_b$ [61]. At t_b we switch off the coupling to the bath and we follow the periodically driven dynamics ($B_0 > 0$) of the isolated system.

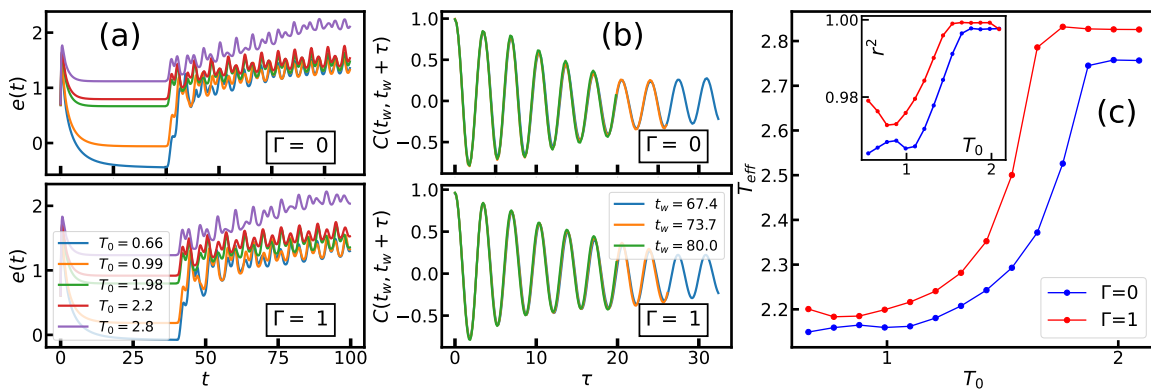


FIG. 2. The classical ($\Gamma = 0$) and quantum ($\Gamma = 1$) PSM. $B_0 = M = J = 1$, $p = 3$, $t_b = 40$ and $\Omega = 1$. (a) The energy density $e(t)$, for several values of the bath temperature T_0 . (b) The symmetric correlation, Eq. (14), evolving from an initial state at temperature $T_0 = 1.98$. (c) The effective temperature T_{eff} against T_0 . The data are obtained through a linear regression of the averaged two-point functions $d\bar{C}(\tau)/d\tau$ and $\bar{R}(\tau)$ from Eqs. (16) and (17), using the classical FDT. The corresponding r^2 parameter is reported in the inset.

In Fig. 2(a) we plot the average energy density $e(t)$ [64] for $\Omega = 1$ and several T_0 . $e(t)$ saturates to a first plateau for $t \lesssim t_b$, signalling that the system reached thermal equilibrium with the bath, and later oscillates around a second one at e_∞ . The latter stroboscopic saturation is compatible with a finite temperature thermalization for both classical and quantum PSM. Like in the lattice ϕ^4 model, the late saturation of $e(t)$ is robust against changes in Ω and the form of the driving force [42].

These results are consistent with the same prethermalization which we also observed in the ϕ^4 . However, we cannot observe deviations of $e(t)$ from e_∞ within our simulation time scales. We also observe that, unlike for the ϕ^4 model, we cannot perform a multi-scale analysis, due to difficulties posed by the spherical constraint. Instead, as we have direct access to the two-point functions, we search for other indications of relaxation to a Gibbs-like state from the Fluctuation-Dissipation Theorem (FDT) [65]. Its classical ($\Gamma = 0$) version states that whenever a system is in equilibrium at temperature T , $dC(\tau)/d\tau = -T R(\tau)$ with $\tau = t - t' > 0$. Although the dynamics are non-stationary due to the driving, C and R exhibit an *approximate* discrete stationarity in the late-time regime, corresponding to the invariance under simultaneous translations of t and t' by the period $2\pi/\Omega$. Motivated by this observation, illustrated in Fig. 2(b), we test the FDT for the averaged two-point functions:

$$\bar{C}(\tau) = \frac{\Omega}{4\pi} \int_{t_0}^{t_0 + \frac{2\pi}{\Omega}} ds [C(s + \tau, s) - m(s + \tau)m(s)] \quad (16)$$

$$\bar{R}(\tau) = \frac{\Omega}{4\pi} \int_{t_0}^{t_0 + \frac{2\pi}{\Omega}} ds R(s + \tau, s), \quad (17)$$

with $m(t) = \int_0^t ds R(t, s)B(s)$ the oscillating magnetization [42]. From the slope of a linear regression of $\bar{R}(\tau)$ against $d\bar{C}(\tau)/d\tau$, we obtain an *effective temperature* T_{eff}

at late times. The T_0 dependence of T_{eff} is displayed, along with the corresponding r^2 parameter from the regression, in Fig. 2(c). The profile of T_{eff} is similar for the classical and quantum cases and resembles the behavior observed in $e_\infty(e_0)$ for the ϕ^4 model. Notably, we find that $r^2 \simeq 1$ for both classical and quantum models, indicating that the classical FDT effectively characterizes the relation between \bar{C} and \bar{R} , even in the latter case.

Discussion and conclusion — In conclusion, our investigation of the dynamics of ergodic systems, with unbounded phase space and driven by a smooth periodic force, revealed clear signatures of prethermalization to a Gibbs-like state. This is indicated either by a saturation of the energy density to a finite value or by the emergence of an approximate fluctuation-dissipation relation. For the ϕ^4 model, we also proposed a perturbative scheme which allowed us to determine the corresponding thermal asymptotic state. Differently from previous studies, prethermalization occurs at all frequencies and the corresponding effective Hamiltonian \mathcal{H}_F is generically distinct from the time-averaged one, $\bar{H}(t)$. A deeper understanding of the connection between \mathcal{H}_F and $\bar{H}(t)$ could be crucial for advancing the experimental realization of long-lived many-body Hamiltonians even at moderate frequencies.

Acknowledgements — We thank D. Abanin, A. Delmonte, A. Polkovnikov and A. Russomanno for discussions. L.C. acknowledges hospitality from the Institute of Physics of Collège de France. L.F.C. acknowledges support from the grant ANR-19-CE30-0014. A.S. acknowledges funding from the grants PNRR MUR project PE0000023-NQSTI and Quanter project Super-Link. M.S. acknowledges funding from the European Research Council (ERC) under the European Union's Horizon 2020 research and innovation programme (Grant agreement No. 101002955 – CONQUER).

-
- [1] P. Kapitza, *Uspekhi Fizicheskikh Nauk* **44**, 7 (1951).
- [2] B. V. Chirikov, *Research concerning the theory of non-linear resonance and stochasticity* (CERN, Geneva, 1971) translated at CERN from the Russian (IYAF-267-TRANS-E).
- [3] S. Fishman, D. R. Grempel, and R. E. Prange, *Phys. Rev. Lett.* **49**, 509 (1982).
- [4] Y. Gefen and D. J. Thouless, *Phys. Rev. Lett.* **59**, 1752 (1987).
- [5] T. Oka and S. Kitamura, *Annu. Rev. Condens. Matter Phys.* **10**, 387 (2019).
- [6] L. D'Alessio and M. Rigol, *Phys. Rev. X* **4**, 041048 (2014).
- [7] A. Lazarides, A. Das, and R. Moessner, *Phys. Rev. E* **90**, 030402 (2014).
- [8] P. Ponte, A. Chandran, Z. Papić, and D. A. Abanin, *Ann. Phys.* **353**, 196 (2015).
- [9] M. Genske and A. Rosch, *Phys. Rev. A* **92**, 062108 (2015).
- [10] V. Khemani, A. Lazarides, R. Moessner, and S. L. Sondhi, *Phys. Rev. Lett.* **116**, 250401 (2016).
- [11] D. V. Else, B. Bauer, and C. Nayak, *Phys. Rev. Lett.* **117**, 090402 (2016).
- [12] N. Y. Yao, A. C. Potter, I.-D. Potirniche, and A. Vishwanath, *Phys. Rev. Lett.* **118**, 030401 (2017).
- [13] A. Russomanno, A. Silva, and G. E. Santoro, *Phys. Rev. Lett.* **109**, 257201 (2012).
- [14] R. Citro, E. G. Dalla Torre, L. D'Alessio, A. Polkovnikov, M. Badii, T. Oka, and E. Demler, *Ann. Phys.* **360**, 694 (2015).
- [15] V. Gritsev and A. Polkovnikov, *SciPost Phys.* **2**, 021 (2017).
- [16] T. Ishii, T. Kuwahara, T. Mori, and N. Hatano, *Phys. Rev. Lett.* **120**, 220602 (2018).
- [17] T. Prosen, *Phys. Rev. Lett.* **80**, 1808 (1998).
- [18] T. Prosen, *J. Phys. A: Math. Gen.* **31**, L645 (1998).
- [19] T. Prosen, *Phys. Rev. E* **60**, 3949 (1999).
- [20] O. Howell, P. Weinberg, D. Sels, A. Polkovnikov, and M. Bukov, *Phys. Rev. Lett.* **122**, 010602 (2019).
- [21] A. Pizzi, A. Nunnenkamp, and J. Knolle, *Phys. Rev. Lett.* **127**, 140602 (2021).
- [22] Y. Sadia, E. G. Dalla Torre, and A. Rajak, *Phys. Rev. B* **105**, 184302 (2022).
- [23] T. Kuwahara, T. Mori, and K. Saito, *Ann. Phys.* **367**, 96 (2016).
- [24] T. Mori, T. Kuwahara, and K. Saito, *Phys. Rev. Lett.* **116**, 120401 (2016).
- [25] D. Abanin, W. D. Roeck, W. W. Ho, and F. Huveneers, *Commun. Math. Phys.* **354**, 809 (2017).
- [26] D. A. Abanin, W. D. Roeck, W. W. Ho, and F. Huveneers, *Phys. Rev. B* **95**, 014112 (2017).
- [27] F. Peronaci, M. Schiró, and O. Parcollet, *Phys. Rev. Lett.* **120**, 197601 (2018).
- [28] F. Peronaci, O. Parcollet, and M. Schiró, *Phys. Rev. B* **101**, 161101 (2020).
- [29] W. W. Ho, T. Mori, D. A. Abanin, and E. G. D. Torre, *Ann. Phys.* **454**, 169297 (2023).
- [30] E. G. D. Torre and D. Dentelski, *SciPost Phys.* **11**, 040 (2021).
- [31] B. Neyenhuis, J. Zhang, P. W. Hess, J. Smith, A. C. Lee, P. Richerme, Z.-X. Gong, A. V. Gorshkov, and C. Monroe, *Sci. Adv.* **3**, e1700672 (2017).
- [32] A. Rubio-Abadal, M. Ippoliti, S. Hollerith, D. Wei, J. Rui, S. L. Sondhi, V. Khemani, C. Gross, and I. Bloch, *Phys. Rev. X* **10**, 021044 (2020).
- [33] P. Peng, C. Yin, X. Huang, C. Ramanathan, and P. Cappellaro, *Nat. Phys.* **17**, 444 (2021).
- [34] C. Shkedrov, M. Menashes, G. Ness, A. Vainbaum, E. Altman, and Y. Sagi, *Phys. Rev. X* **12**, 011041 (2022).
- [35] W. Hodson and C. Jarzynski, *Phys. Rev. Res.* **3**, 013219 (2021).
- [36] A. Rajak, R. Citro, and E. G. D. Torre, *J. Phys. A: Math. Theor.* **51**, 465001 (2018).
- [37] A. Rajak, I. Dana, and E. G. D. Torre, *Phys. Rev. B* **100**, 100302(R) (2019).
- [38] T. Mori, T. N. Ikeda, E. Kaminishi, and M. Ueda, *J. Phys. B: At. Mol. Opt.* **51**, 112001 (2018).
- [39] S. A. Weidinger and M. Knap, *Sci. Rep.* **7**, 45382 (2017).
- [40] G. Parisi, *Europhysics Letters (EPL)* **40**, 357 (1997).
- [41] G. Aarts, G. F. Bonini, and C. Wetterich, *Nucl. Phys. B* **587**, 403 (2000).
- [42] See Supplemental Material.
- [43] M. Pettini and M. Cerruti-Sola, *Phys. Rev. A* **44**, 975 (1991).
- [44] M. Pettini, *Phys. Rev. E* **47**, 828 (1993).
- [45] E. Shimshoni, G. Morigi, and S. Fishman, *Phys. Rev. Lett.* **106**, 010401 (2011).
- [46] P. Silvi, G. D. Chiara, T. Calarco, G. Morigi, and S. Montangero, *Ann. Phys.* **525**, 827 (2013).
- [47] P. Silvi, T. Calarco, G. Morigi, and S. Montangero, *Phys. Rev. B* **89**, 094103 (2014).
- [48] L. Landau and E. Lifshitz, *Mechanics* (Elsevier, 1976).
- [49] Notice that this is not the high-frequency limit, which instead would require $\Omega \sim O(1)$ and $\omega_0^2 \sim \epsilon$, instead of the scaling $\Omega^2 \sim \omega_0^2 + O(\epsilon)$ considered here.
- [50] C. M. Bender and S. A. Orszag, *Advanced Mathematical Methods for Scientists and Engineers I* (Springer New York, 1999).
- [51] S. Rahav, I. Gilary, and S. Fishman, *Phys. Rev. A* **68**, 013820 (2003).
- [52] In terms of the new variables \mathbf{u} and \mathbf{v} , H_{ϕ^4} coincides with $\mathcal{H}_0(\mathbf{u}, \mathbf{v})$ at the leading order in ϵ .
- [53] J. M. Kosterlitz, D. J. Thouless, and R. C. Jones, *Phys. Rev. Lett.* **36**, 1217 (1976).
- [54] L. F. Cugliandolo, D. R. Grempel, and C. A. da Silva Santos, *Phys. Rev. Lett.* **85**, 2589 (2000).
- [55] L. F. Cugliandolo, D. R. Grempel, and C. A. da Silva Santos, *Phys. Rev. B* **64**, 014403 (2001).
- [56] L. F. Cugliandolo and G. Lozano, *Phys. Rev. B* **59**, 915 (1999).
- [57] S. Bera, K. Y. Venkata Lokesh, and S. Banerjee, *Phys. Rev. Lett.* **128**, 115302 (2022).
- [58] T. Anous and F. M. Haehl, *J. Stat. Mech.* **2021**, 113101 (2021).
- [59] M. Winer, R. Barney, C. L. Baldwin, V. Galitski, and B. Swingle, *J. High Energy Phys.* **2022**, 32 (2022).
- [60] L. Correale, A. Polkovnikov, M. Schiró, and A. Silva, *SciPost Phys.* **15**, 190 (2023).
- [61] S. Thomson, P. Urbani, and M. Schiró, *Phys. Rev. Lett.* **125**, 120602 (2020).
- [62] L. Berthier, L. F. Cugliandolo, and J. L. Iguain, *Phys. Rev. E* **63**, 051302 (2001).
- [63] G. Busiello, R. V. Saburova, V. G. Sushkova, and G. P. Chugunova, *Phys. Solid State* **46**, 316 (2004).
- [64] $\lim_{N \rightarrow \infty} e(t)$ can be expressed in terms of $C(t, t')$ and

- $R(t, t')$ (see SM [42]).
- [65] J. K. Nielsen and J. C. Dyre, Phys. Rev. B **54**, 15754 (1996).
- [66] D. N. Joanes and C. A. Gill, Journal of the Royal Statistical Society: Series D (The Statistician) **47**, 183–189 (1998).
- [67] L. F. Cugliandolo, G. S. Lozano, and E. N. Nessi, J. Stat. Mech. **2017**, 083301 (2017).
- [68] A. Kamenev, *Field Theory of Non-Equilibrium Systems* (Cambridge University Press, 2011).
- [69] A. Haldar, P. Haldar, S. Bera, I. Mandal, and S. Banerjee, Phys. Rev. Res. **2**, 013307 (2020).

Supplemental Material: Finite-frequency prethermalization in periodically driven ergodic systems

In Section 1, we show that the driven dynamics of the classical one-dimensional lattice ϕ^4 model deviates from its prethermal plateau when integrated at longer times and discuss the dependence of prethermalization on the degree of non-linearity in the system. In Section 2, we provide a comprehensive exposition of the multiple-scale analysis, applied to the lattice ϕ^4 model. In Section 3, we write down and derive explicitly the mode coupling equations, which govern the dynamics of the correlation and response functions, in the thermodynamic limit of the p -spin spherical model. In Section 4, we discuss the ergodic properties of both the two models, in absence of a time-dependent drive. Finally, in Section 5, we study the Floquet dynamics of both models, driven by smooth periodic forces different from the ones considered in the Letter.

1. Deviations from the prethermal plateau in the classical lattice ϕ^4 model

In this section, we extend the integration of Eqs. (19) over a longer time scale to investigate the behavior of the classical lattice ϕ^4 model. We compute the resulting average energy density $e(t) = \langle H_{\phi^4}(\mathbf{x}(t), \dot{\mathbf{x}}(t)) \rangle_0 / N$, where $H_{\phi^4}(\mathbf{x}(t), \mathbf{p}(t))$ is defined in Eq. (1) of the Letter. As in the Letter, the initial condition is chosen as ensemble of microcanonical configurations, sampled from the surface $H_{\phi^4}(\mathbf{x}(0), \dot{\mathbf{x}}(0)) = Ne_0$ for a fixed initial energy density e_0 . To integrate up to a larger maximum time, we fix \mathcal{N} to a smaller value than in the Letter. We integrate the dynamics for different values of λ , the parameter controlling the non-linearity of the system. From Fig. 3-(a), it is already evident that the energy density $e(t)$ displays deviations from its finite plateau at e_∞ at sufficiently long-time, confirming the prethermal nature of the plateau. We also observe that the height of the plateau increases by decreasing λ .

To qualitatively assess the influence of the non-linearity on the prethermal plateau, we introduce the normalized quantity

$$Q(t) = \frac{e(t) - e_0}{e_\infty - e_0}, \quad (18)$$

which saturates to 1 when $e(t)$ saturates to e_∞ and such that $Q(0) = 0$. Here, we estimate e_∞ as $e(t = t_0)$ for a fixed intermediate time t_0 . As depicted in Fig. 3-(b), deviations of $Q(t)$ from its plateau appear at earlier times as λ increases, suggesting that a stronger non-linearity suppresses prethermalization.

2. Detailed calculations on multiple-scale analysis

In this section, we aim to provide a review on the multiple-scale analysis (MSA) that we employed in the Letter. We will focus again on the Hamilton dynamics of the classical lattice ϕ^4 model, governed by the equations

$$\ddot{x}_i + \omega_0^2 x_i + \lambda x_i^3 = B_0 \sin(\Omega t) + g (x_{i+1} - 2x_i + x_{i-1}), \quad (19)$$

for $i = 1 \dots N$. We rescale the model parameters as $B_0 = \epsilon \tilde{B}_0$, $\lambda = \epsilon \tilde{\lambda}$ and $g = \epsilon \tilde{g}$. We also rescale the harmonic coupling as $\omega_0^2 = \Omega^2 - \epsilon \Delta \omega^2$. We will work in the limit of small ϵ , while keeping all other parameters of order one. As outlined in the Letter, the starting point of the MSA consists in introducing a redundant time variable $\tau = \epsilon t$. τ defines a long time scale, since it becomes significant only when t is of order ϵ^{-1} or larger. Although we expect that the actual solution $\mathbf{x}(t)$ to Eq. (19) is a function of t alone, MSA seeks solutions which are functions of both variables

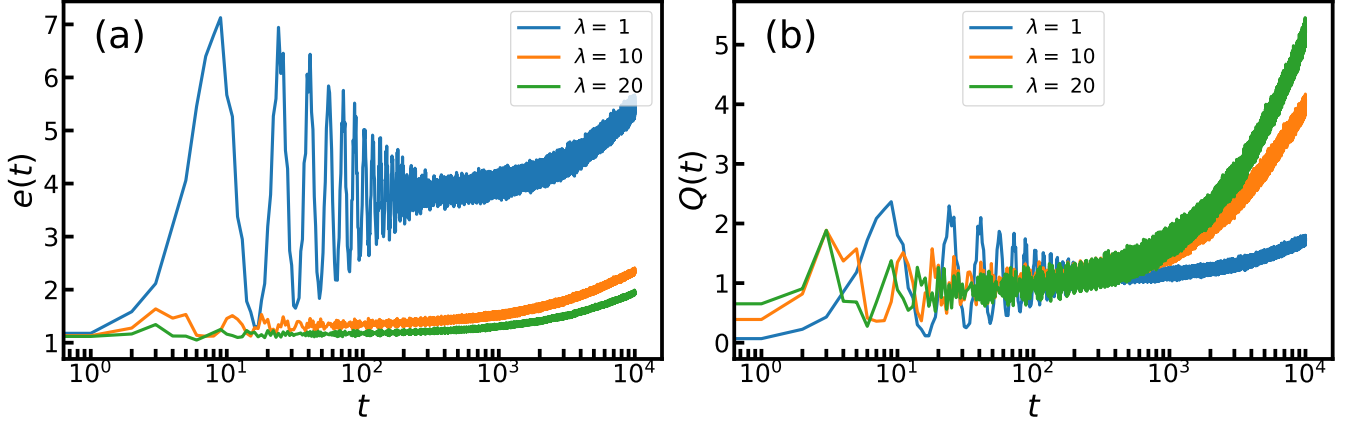


FIG. 3. Average energy densities for the one dimensional lattice ϕ^4 model, evolving from Eqs. (87), with $N = 100$. Data are averaged over $\mathcal{N} = 50$ configurations. Other parameters are set as $\omega_0^2 = B_0 = g = 1$, $e_0 = 1$ and $\Omega = 2$. (a) $e(t) = \langle H_{\phi^4}(\mathbf{x}(t), \mathbf{p}(t)) \rangle_0 / N$. (b) $Q(t)$ from Eq. (18). We estimate e_∞ as $e(t_0 = 100)$.

t and τ , treated as independent from each other. Such expression of $\mathbf{x}(t)$ as a function of two variables is an artifice to remove secular effects; the actual solution has t and τ related by $\tau = \epsilon t$. The formal procedure consists in assuming a perturbative expansion in powers of ϵ :

$$x_i(t) = x_{0,i}(t, \tau) + \epsilon x_{1,i}(t, \tau) + \dots, \quad (20)$$

for small ϵ . We use the chain rules $d/dt = \partial_t + \epsilon \partial_\tau$ for partial differentiation to compute the derivatives of the variables $x_i(t)$, obtaining

$$\frac{dx_i}{dt} = \frac{\partial x_{0,i}}{\partial t} + \epsilon \left(\frac{\partial x_{1,i}}{\partial t} + \frac{\partial x_{0,i}}{\partial \tau} \right) + O(\epsilon^2) \quad (21)$$

and

$$\frac{d^2 x_i}{dt^2} = \frac{\partial^2 x_{0,i}}{\partial t^2} + \epsilon \left(\frac{\partial^2 x_{1,i}}{\partial t^2} + 2 \frac{\partial^2 x_{0,i}}{\partial t \partial \tau} \right) + O(\epsilon^2). \quad (22)$$

By substituting Eq. (22) in Eq. (19) and collecting powers of ϵ , we deduce

$$\frac{\partial^2 x_{0,i}}{\partial t^2} + \Omega^2 x_{0,i} = 0, \quad (23)$$

$$\frac{\partial^2 x_{1,i}}{\partial t^2} + \Omega^2 x_{1,i} = -2 \frac{\partial^2 x_{0,i}}{\partial t \partial \tau} + \Delta \omega^2 x_{0,i} + \tilde{g}(x_{0,i+1} - 2x_{0,i} + x_{0,i-1}) - \tilde{\lambda} x_{0,i}^3 + \tilde{B}_0 \sin(\Omega t). \quad (24)$$

The general solution to Eq. (23) is

$$x_{0,i}(t, \tau) = A_i(\tau) e^{i\Omega t} + A_i^*(\tau) e^{-i\Omega t}. \quad (25)$$

By plugging this expression into Eq. (24), we derive

$$\frac{\partial^2 x_{1,i}}{\partial t^2} + \Omega^2 x_{1,i} = 2 \operatorname{Re} \left[e^{i\Omega t} \left(-2i\Omega \frac{dA_i}{d\tau} + \Delta \omega^2 A_i + \tilde{g}(A_{i+1} - 2A_i + A_{i-1}) - 3\tilde{\lambda} A_i^2 A_i^* - \frac{i}{2} \tilde{B}_0 \right) - \tilde{\lambda} e^{i3\Omega t} A_i^3 \right]. \quad (26)$$

The slowly varying amplitude $A_i(\tau)$ and its complex conjugate $A_i^*(\tau)$ are determined by imposing that secular terms, proportional either to $e^{i\Omega t}$ or $e^{-i\Omega t}$, do not appear in the next order, that is on the right-hand-side of Eq. (24), as these would predict a divergence which we do not observe in the complete numerical solution of this problem. The vanishing of such secular terms thus leads to the following equation of motion for $A_i(\tau)$:

$$\frac{dA_i}{d\tau} = \frac{1}{2i\Omega} \left[\Delta \omega^2 A_i - 3\tilde{\lambda} A_i^2 A_i^* - \frac{i}{2} \tilde{B}_0 + \tilde{g}(A_{i+1} - 2A_i + A_{i-1}) \right]. \quad (27)$$

The equation of motion for $A_i^*(\tau)$ is just the complex conjugate of Eq. (27). We rewrite Eq. (27) in terms of the coordinates $u_i(\tau) = A_i(\tau) + A_i^*(\tau)$ and $v_i(\tau) = [A_i(\tau) - A_i^*(\tau)]/i$, which consequently obey the equations:

$$\begin{cases} \frac{du_i}{d\tau} = \frac{1}{2\Omega} \left[\Delta\omega^2 v_i + \tilde{g}(v_{i+1} - 2v_i + v_{i-1}) - \frac{3}{4}\tilde{\lambda}(u_i^2 + v_i^2)v_i - \tilde{B}_0 \right], \\ \frac{dv_i}{d\tau} = \frac{1}{2\Omega} \left[-\Delta\omega^2 u_i - \tilde{g}(u_{i+1} - 2u_i + u_{i-1}) + \frac{3}{4}\tilde{\lambda}(u_i^2 + v_i^2)u_i \right]. \end{cases} \quad (28)$$

In terms of $u_i(\tau)$ and $v_i(\tau)$, the leading order solution, which satisfies Eq. (23), reads $x_{0,i}(t) = u_i(\tau) \cos(\Omega t) + v_i(\tau) \sin(\Omega t)$. The system of Eqs. (28) is Hamiltonian, as it can be rewritten as

$$\begin{cases} \frac{du_i}{d\tau} = -\frac{\partial \mathcal{H}_F}{\partial v_i}, \\ \frac{dv_i}{d\tau} = \frac{\partial \mathcal{H}_F}{\partial u_i}, \end{cases} \quad (29)$$

with the many-body effective Hamiltonian:

$$\mathcal{H}_F(\mathbf{u}, \mathbf{v}) = \frac{1}{2\Omega} \sum_i \left\{ -\frac{\Delta\omega^2}{2}(u_i^2 + v_i^2) + \frac{\tilde{g}}{2}[(u_{i+1} - u_i)^2 + (v_{i+1} - v_i)^2] + \frac{3\tilde{\lambda}}{16}(u_i^2 + v_i^2)^2 + \tilde{B}_0 v_i \right\}.$$

3. Dynamical equations for the correlation and response function in the p-spin spherical model

The aim of this section is to derive and discuss the closed set of equations of motions governing the dynamics of the correlation and response functions, $C(t, t')$ and $R(t, t')$, of the p -spin spherical model (PSM) investigated in the Letter. We anticipate that, in analogy to the results obtained in Refs. [62, 63], which studied the periodically driven dynamics of the PSM coupled to a thermal bath, the equations describing its Floquet dynamics have Schwinger-Dyson structure and are given by

$$[M\partial_t^2 + z(t)]R(t, t') = \delta(t - t') + \int_0^t dt'' \Sigma(t, t'')R(t'', t'),$$

$$[M\partial_t^2 + z(t)]C(t, t') = \int_0^t dt'' \Sigma(t, t'')C(t'', t') + \int_0^{t'} dt'' D(t, t'')R(t', t'') +$$

$$+ B(t) \int_0^{t'} dt'' R(t', t'')B(t''). \quad (30)$$

We will define the self-energy $\Sigma(t, t')$ and the vertex $D(t, t')$ later on in this section. The time-dependent Lagrange multiplier $z(t)$ enforces the spherical constraint and has an expression in terms of C and R as well. In the Letter, we integrate numerically Eqs. (30) and (31) to compute the correlation and response function, evolving from the equal-time conditions:

$$C(t, t) = 1, \quad \partial_t C(t, t')|_{t' \rightarrow t^-} = \partial_t C(t, t')|_{t' \rightarrow t^+} = 0, \quad (32)$$

$$R(t, t) = 0, \quad \partial_t R(t, t')|_{t' \rightarrow t^-} = \frac{1}{M}, \quad \partial_t R(t, t')|_{t' \rightarrow t^+} = 0, \quad (33)$$

resulting from the spherical constraint and the causal structure of the response function. Then, following Refs. [61, 67], we compute the energy density of the system as

$$e(t) = -\frac{M}{2} \partial_t^2 C(t, t')|_{t' \rightarrow t^-} - \frac{1}{p} \int_0^t dt'' [\Sigma(t, t'')C(t, t'') + D(t, t'')R(t, t'')]. \quad (34)$$

This section is organized as follows. In Section , we derive Eqs. (30) and (31) using the Schwinger-Keldysh formalism in the large N limit. In Section , we show how to determine the Lagrange multiplier $z(t)$ explicitly, in terms of the correlation and response functions. Finally, in Section , we discuss the predictor-corrector algorithm, that we use to integrate Eqs. (30) and (31) numerically.

3.1 Derivation of the Schwinger-Dyson equations

We begin by reminding that the Hamiltonian of the driven quantum PSM is defined as

$$\hat{H}_J = \frac{1}{2M} \sum_{i=1}^N \hat{\Pi}_i^2 - \mathcal{J}(t) \sum_{i_1 < \dots < i_p} J_{i_1, \dots, i_p} \hat{\sigma}_{i_1} \cdots \hat{\sigma}_{i_p} - B(t) \sum_i \hat{\sigma}_i \quad (35)$$

with all-to-all couplings J_{i_1, \dots, i_p} , independently sampled from a Gaussian distribution with zero mean and variance $\overline{J^2} = 2J^2 p! / N^{p-1}$. The spins $\hat{\sigma}_i$ obey the usual spherical constraint $\sum_i \langle \hat{\sigma}_i^2 \rangle = N$ (on average). The canonical commutation relations $[\hat{\sigma}_j, \hat{\Pi}_k] = i\hbar \delta_{jk}$ hold. We added a time-dependent factor $\mathcal{J}(t)$ to allow for other kinds of drives.

The unitary dynamics generated by the Hamiltonian in Eq. (35) can be expressed through a path integral on the Schwinger-Keldysh contour [68], whose generating functional reads

$$\mathcal{Z}[J] = \int \mathcal{D}\sigma^+ \mathcal{D}\sigma^- \exp [i (S[\sigma^+] - S[\sigma^-]) / \hbar] \langle \sigma^+ | \hat{\rho}(0) | \sigma^- \rangle. \quad (36)$$

Here, $\hat{\rho}(0)$ represents the element of the initial density matrix at $t = 0$ and is chosen to be a random infinite-temperature initial state, which is uncorrelated with the disorder. The last factor in the path integral is then just an irrelevant factor. The action S can be defined in terms of a quadratic term S_0 and a disordered interaction term $V_J(\sigma)$ as follows:

$$S[\sigma, J] = S_0[\sigma] - \int_0^\infty dt \mathcal{J}(t) V_J(\sigma(t)), \quad (37)$$

$$S_0[\sigma] = \int_0^\infty dt \left[\frac{M}{2} \dot{\sigma}^2 - \frac{z(t)}{2} (\sigma^2 - N) \right] - \sum_{i=1}^N \int_0^\infty dt B(t) \sigma_i(t), \quad (38)$$

$$V_J(\sigma) = - \sum_{i_1 < \dots < i_p}^N J_{i_1 \dots i_p} \sigma_{i_1} \cdots \sigma_{i_p}. \quad (39)$$

The quadratic part S_0 contains a kinetic term, chosen such that the eventual dynamical equations are written in terms of second derivatives with respect to time. The time-dependent Lagrange multiplier $z(t)$ enforces the constraint $\sum_i^N \sigma_i^2 = N$. We also included in S_0 the coupling to the time-dependent field $B(t)$. This action can be split into components σ^+ and σ^- residing on the forward and backwards Keldysh contours respectively, and recast as

$$S[\sigma^+, \sigma^-, J] = S_0[\sigma^+] - S_0[\sigma^-] - \int_0^\infty dt \mathcal{J}(t) [V_J(\sigma^+(t)) - V_J(\sigma^-(t))] \quad (40)$$

where the relative minus sign comes from reversing the integration limits on the reverse contour.

System-Bath Coupling

The coupling between the system and bath can be treated exactly as in Ref. [56]. We couple the quantum p -spin Hamiltonian linearly to a bath of harmonic oscillators, assumed to be in thermal equilibrium, for a time window $[0, t_b]$. This coupling can be described by the functional [68]:

$$S_{bath} = \int_0^{t_b} dt \int_0^{t_b} dt' \left\{ - [\sigma^+(t) - \sigma^-(t)] \eta(t-t') [\sigma^+(t') + \sigma^-(t')] \right. \\ \left. + i [\sigma^+(t) - \sigma^-(t)] \nu(t-t') [\sigma^+(t') - \sigma^-(t')] \right\} \quad (41)$$

where η and ν are the correlation and response functions of the bath, and are time-translation invariant due to the bath being in equilibrium. They are given by

$$\eta(t-t') = -\Theta(t-t') \int_0^\infty d\omega I(\omega) \sin[\omega(t-t')], \quad (42)$$

$$\nu(t-t') = \int_0^\infty I(\omega) \coth\left(\frac{1}{2}\beta\hbar\omega\right) \cos[\omega(t-t')], \quad (43)$$

where $I(\omega)$ is the spectral function of the bath. We choose an Ohmic bath with $I(\omega) = \frac{1}{\pi} \exp(-|\omega|/\Lambda)$ and set the integration cutoff to be $\Lambda = 5$.

Disorder Averaging

For an initial condition $\hat{\rho}(0)$ uncorrelated with the disorder, we can perform the disorder average explicitly. As in the Letter, we assume that the distribution of the disorder variable $J_{i_1 \dots i_p}$ is given by the Gaussian distribution

$$P[J] = \sqrt{\frac{N^{p-1}}{\pi p! J^2}} \exp\left(-\frac{N^{p-1}}{p! J^2} \sum_{i_1 \neq \dots \neq i_p} (J_{i_1 \dots i_p})^2\right) \quad (44)$$

with zero average and variance $\overline{(J_{i_1 \dots i_p})^2} = (p! J^2)/(2N^{p-1})$. The disorder average reduces to just averaging over the terms including the $V_J(\boldsymbol{\sigma})$, which are the only ones depending on the disorder. By an straightforward calculation, we obtain the disorder-averaged generating functional:

$$\overline{\mathcal{Z}[J]} = \int \mathcal{D}\sigma^- \mathcal{D}\sigma^+ \exp\left[i(S_{\text{eff}}[\boldsymbol{\sigma}^+, \boldsymbol{\sigma}^-])/\hbar\right]. \quad (45)$$

The effective action at the exponent is given by:

$$S_{\text{eff}}[\boldsymbol{\sigma}^+, \boldsymbol{\sigma}^-] = S_0[\boldsymbol{\sigma}^+] - S_0[\boldsymbol{\sigma}^-] - V_D[\boldsymbol{\sigma}^+, \boldsymbol{\sigma}^-] + S_{\text{bath}}[\boldsymbol{\sigma}^+, \boldsymbol{\sigma}^-], \quad (46)$$

$$V_D[\boldsymbol{\sigma}^+, \boldsymbol{\sigma}^-] = \frac{iN}{4} \int dt dt' \mathcal{J}(t) \mathcal{J}(t') J^2 \sum_{\alpha, \beta = \pm} \sum_{i=1}^N \alpha \beta \left(\frac{1}{N} \sigma_i^\alpha(t) \sigma_i^\beta(t')\right)^p \quad (47)$$

where $\alpha, \beta = \pm$ are the Schwinger-Keldysh contours.

Transformed Order Parameters

The contribution to the action containing at most quadratic terms in the spins $\sigma_i^\alpha(t)$ can be written down as:

$$\frac{1}{\hbar} S_{\text{eff}}^{(2)}[\boldsymbol{\sigma}^+, \boldsymbol{\sigma}^-] = -\frac{1}{2} \sum_{i, \alpha, \beta} \int dt dt' \sigma_i^\alpha(t) O_p^{\alpha\beta}(t, t') \sigma_i^\beta(t') - \sum_{i, \alpha} \int \frac{dt}{\hbar} \alpha B(t) \sigma_i^\alpha(t), \quad (48)$$

where again $\alpha, \beta = \pm$. The matrix elements $O_p^{\alpha\beta}(t, t')$, appearing in Eq. (48), are explicitly given by

$$O_p^{++}(t, t') = \frac{1}{\hbar} [M \partial_t^2 + z^+(t)] \delta(t - t') - \frac{2}{\hbar} (i\nu(t - t') - \eta(t - t')) \Theta(t - t_b) \Theta(t' - t_b), \quad (49)$$

$$O_p^{+-}(t, t') = \frac{1}{\hbar} (2\eta(t - t') + 2i\nu(t - t')) \Theta(t - t_b) \Theta(t' - t_b), \quad (50)$$

$$O_p^{-+}(t, t') = \frac{1}{\hbar} (-2\eta(t - t') + 2i\nu(t - t')) \Theta(t - t_b) \Theta(t' - t_b), \quad (51)$$

$$O_p^{--}(t, t') = -\frac{1}{\hbar} [M \partial_t^2 + z^-(t)] \delta(t - t') - \frac{2}{\hbar} (i\nu(t - t') + \eta(t - t')) \Theta(t - t_b) \Theta(t' - t_b). \quad (52)$$

Saddle-Point Equations

To decouple the p -body interaction term, we introduce a new set of variables $Q^{\alpha\beta}(t, t')$, by using the following trivial representation of the number 1:

$$1 = \int \prod_{\alpha\beta} \mathcal{D}Q^{\alpha\beta} \delta\left(\frac{1}{N} \boldsymbol{\sigma}^\alpha(t) \boldsymbol{\sigma}^\beta(t') - Q^{\alpha\beta}(t, t')\right), \quad (53)$$

$$\propto \int \prod_{\alpha\beta} \mathcal{D}Q^{\alpha\beta} \mathcal{D}\lambda^{\alpha\beta} \exp\left(-\frac{i}{2} \lambda^{\alpha\beta} (\boldsymbol{\sigma}^\alpha(t) \boldsymbol{\sigma}^\beta(t') - N Q^{\alpha\beta}(t, t'))\right). \quad (54)$$

Then, using a compact notation, the final form of the generating functional is

$$\overline{\mathcal{Z}[J]} = \int \mathcal{D}Q \mathcal{D}\lambda \exp\{NS[Q, \lambda]\} \quad (55)$$

where

$$S[Q, \lambda] = \sum_{\alpha\beta} \int dt dt' \left\{ \frac{i}{2} \lambda^{\alpha\beta}(t, t') Q^{\alpha\beta}(t, t') - \frac{1}{4} Q_{\alpha\beta}(t, t') \right\} + \log Z[Q, \lambda] \quad (56)$$

and

$$Z[Q, \lambda] = \int \mathcal{D}\sigma^- \mathcal{D}\sigma^+ \exp \left\{ -\frac{1}{2} \sum_{\alpha\beta} \int dt dt' \sigma^\alpha(t) [iO_p^{\alpha\beta}(t, t') + i\lambda^{\alpha\beta}(t, t')] \sigma^\beta(t') + \right. \\ \left. - i \sum_\alpha \int \frac{dt}{\hbar} \alpha B(t) \sigma_i^\alpha(t) \right\} \quad (57)$$

is the action of a single effective spin. Then, defining the matrix $M^{\alpha\beta}(t, t') = iO_p^{\alpha\beta}(t, t') + i\lambda^{\alpha\beta}(t, t')$, the saddle point equations for the $N \rightarrow \infty$ limit read

$$Q^{\alpha\beta}(t, t') = \langle \sigma^\alpha(t) \sigma^\beta(t') \rangle = (M^{-1})^{\alpha\beta}(t, t') + m(t)m(t') \quad (58)$$

$$i\lambda^{\alpha\beta}(t, t') = \frac{p}{2} F[Q]^{\alpha\beta}(t, t') \quad (59)$$

The average $\langle \dots \rangle$ in Eq. (58) is performed over the partition function $Z[Q, \lambda]$ and the magnetization,

$$m(t) = \langle \sigma(t) \rangle = \sum_\beta \int dt' \frac{i}{\hbar} (M^{-1})^{\alpha\beta}(t, t') \beta B(t') , \quad (60)$$

does not actually depend on the Keldysh index α , like every other one-time quantity. The matrices used in Eq. (58) are defined as

$$\mathcal{Q}(t, t') = \begin{bmatrix} Q^{++}(t, t') & Q^{+-}(t, t') \\ Q^{-+}(t, t') & Q^{--}(t, t') \end{bmatrix}, \quad \mathcal{M}(t, t') = \begin{bmatrix} M^{++}(t, t') & M^{+-}(t, t') \\ M^{-+}(t, t') & M^{--}(t, t') \end{bmatrix} \quad (61)$$

$$F[Q](t, t') = \begin{bmatrix} [Q^{++}(t, t')]^{p-1} & -[Q^{+-}(t, t')]^{p-1} \\ -[Q^{-+}(t, t')]^{p-1} & [Q^{--}(t, t')]^{p-1} \end{bmatrix} \frac{\mathcal{J}(t)\mathcal{J}(t')\mathcal{J}^2}{\hbar^2} \quad (62)$$

We used the same notation of Ref. [56]. Manipulating Eq. (58), we can rewrite the response function as

$$R(t, t') = \frac{i}{\hbar} [Q^{++}(t, t') - Q^{+-}(t, t')] = \frac{i}{\hbar} [(M^{-1})^{++}(t, t') - (M^{-1})^{+-}(t, t')] . \quad (63)$$

Then, by fixing $\alpha = +1$ in Eq. (60), the magnetization becomes

$$m(t) = \int dt' R(t, t') B(t') . \quad (64)$$

Using Eq. (59) and applying the matrix \mathcal{M} on both sides of Eq. Eq. (58), we obtain the dynamical equations for all the two-point correlators on the Keldysh contour, represented in the following compact form:

$$iO_p \otimes \mathcal{Q}(t, t') = \mathcal{I} - \frac{p}{2} F[Q] \otimes \mathcal{Q}(t, t') + \mathcal{S} B(t) \langle \sigma(t') \rangle \quad (65)$$

where the matrix elements $\mathcal{S}^{\alpha\beta} = \alpha$ do not depend on the time indices.

Dynamical Equations

Following the same prescription described in Ref. [56], it is straightforward to obtain a closed set of dynamical equations for the response function $R(t, t')$ and the (symmetric) correlation function

$$C(t, t') = \frac{1}{2} [Q^{+-}(t, t') + Q^{-+}(t, t')] . \quad (66)$$

In particular, the equations of motion for the response function $R(t, t')$ are obtained by taking the difference of the $++$ and $+-$ components of Eq. (65), while the ones for $C(t, t')$ are obtained by taking the addition of the $+-$ and $-+$ components. After some algebra, the result is given by:

$$[M\partial_t^2 + z(t)]R(t, t') = \delta(t - t') + \int_0^t dt'' \Sigma(t, t'')R(t'', t') , \quad (67)$$

$$[M\partial_t^2 + z(t)]C(t, t') = \int_0^t dt'' \Sigma(t, t'')C(t'', t') + \int_0^{t'} dt'' D(t, t'')R(t', t'') + , \quad (68)$$

$$+ B(t) \int_0^{t'} dt'' R(t', t'')B(t'') .$$

Here, we have defined the self-energy $\Sigma(t, t')$ and the vertex $D(t, t')$ as

$$\Sigma(t, t') = -4\eta(t - t')\Theta(t_b - t)\Theta(t_b - t') + \quad (69)$$

$$- \frac{p\mathcal{J}(t)\mathcal{J}(t')J^2}{\hbar} \text{Im} \left[C(t, t') - \frac{i\hbar}{2} R(t, t') \right]^{p-1} ,$$

$$D(t, t') = 2\hbar\nu(t - t')\Theta(t_b - t)\Theta(t_b - t') + \quad (70)$$

$$+ \frac{p\mathcal{J}(t)\mathcal{J}(t')J^2}{2} \text{Re} \left[C(t, t') - \frac{i}{2} (\hbar R(t, t') + \hbar R(t', t)) \right]^{p-1} .$$

This result is exactly the one that we anticipated at the beginning of Section 3, now with explicit functional forms for the two kernels.

The equations for the classical PSM can be readily obtained from the ones above by simply taking the $\hbar \rightarrow 0$ limit. The global structure of the equations is the same, only the Σ and D kernels are affected and considerably simplified.

3.2 The evolution equation for the Lagrange multiplier

In this section we discuss how to self-consistently determine the Lagrange multiplier $z(t)$. The approach typically used in the literature [56] consists in evaluating Eqs. (30) and (31) at equal times $t' = t$:

$$z(t) = \int_0^t dt'' \left[\Sigma(t, t'')C(t'', t) + D(t, t'')R(t, t'') \right] - M\partial_t^2 C(t, t') \Big|_{t' \rightarrow t} . \quad (71)$$

We observe that Eq. (71) leads to ambiguities, as it tautologically depends on the second derivative of $C(t, t')$ at equal times. This issue is irrelevant while the system is coupled to a thermal bath [56], which naturally leads $z(t)$ to thermalize, or when the total energy is conserved, as the second derivative can be replaced by a causal expression containing the conserved energy density [61, 67]. However, for $t > t_b$ none of these two condition is met in our protocol, as the system evolves under a unitary dynamics generated by a time-dependent Hamiltonian. In this case, Eq. (71) does not determine $z(t)$. Here we solve this issue by determining $z(t)$ from the spherical constraint, according to the following procedure. We take the total derivative of the constraint equation $C(t, t) = 1$ multiple times and obtain:

$$0 = \frac{d}{dt} C(t, t) = \lim_{t' \rightarrow t} \partial_t C(t, t') ,$$

$$0 = \frac{d^2}{dt^2} C(t, t) = \lim_{t' \rightarrow t} [\partial_t^2 C(t, t') + \partial_t \partial_{t'} C(t, t')] , \quad (72)$$

$$0 = \frac{d^3}{dt^3} C(t, t) = \lim_{t' \rightarrow t} [\partial_t^3 C(t, t') + 3\partial_t^2 \partial_{t'} C(t, t')] .$$

We used a compact notation $\partial_t = d/dt$ and we also used the symmetry relation $C(t, t') = C(t', t)$ in the last equality of each line of Eqs. (72). It is easy to realize that the first line of Eqs. (72) corresponds to some of the equal-time conditions described in Eqs. (33) and that the second line is useless, as $\partial_t \partial_{t'} C(t, t')$ cannot be computed using the dynamical equations. The third line is instead the one that we use to determine $z(t)$. Specifically, we observe that

the right-hand-side of its second equality can be rewritten in terms of partial derivatives, performed with respect to t and t' respectively, of both sides of Eq. (31). After some algebra, we obtain

$$\begin{aligned} \frac{dz}{dt} = & \int_0^t dt'' \left[\partial_t \Sigma(t, t'') C(t, t'') + \partial_t D(t, t'') R(t, t'') + 3\Sigma(t, t'') \partial_t C(t, t'') + 3D(t, t'') \partial_t R(t, t'') \right] + \\ & + \partial_t B(t) \int_0^t dt'' R(t, t'') B(t'') + 3B(t) \int_0^t dt'' \partial_t R(t, t'') B(t'') \end{aligned} \quad (73)$$

From Eq. (73) it is easy to determine the Lagrange multiplier in a causal form, as

$$\begin{aligned} z(t) = & \int_{t_0}^t dt' \int_0^{t'} dt'' \left[\partial_{t'} \Sigma(t', t'') C(t, t'') + \partial_{t'} D(t', t'') R(t', t'') + 3\Sigma(t', t'') \partial_{t'} C(t', t'') + 3D(t', t'') \partial_{t'} R(t', t'') \right] + \\ & + \int_{t_0}^t dt' \int_0^{t'} dt'' \left[\partial_{t'} B(t') R(t, t'') B(t'') + 3B(t') \partial_{t'} R(t', t'') B(t'') \right] + z(t_0) \end{aligned} \quad (74)$$

provided that we can access the value $z(t_0)$, for some t_0 . Thus we first solve numerically the dissipative dynamics generated from Eqs. (30) and (31), for $0 < t < t_b$, using the standard expression from Eq. (71). Subsequently, we solve the ‘‘closed dynamics’’ for $t > t_b$ using the expression from Eq. (74) for $t_0 = t_b$ and by using the knowledge of $z(t_b)$ that we obtained by integrating the dissipative dynamics.

3.3 Predictor-corrector scheme for the Mode-Coupling equations

To solve Eqs. (30) and (31) in the Letter, we first introduce a discrete time step Δt and we discretize the times as $t = n\Delta t$, $t' = m\Delta t$, etc. for n and m non-negative integers. We use a ‘‘forward’’ discretization scheme for the time derivatives, that is

$$\partial_t f(t, t') \approx (f_{n+1, m} - f_{n, m}) / \Delta t, \quad (75)$$

for every two-point function $f(t, t')$. With this notation, the discretized version of Eqs. (30) and (31) equations is

$$\begin{cases} R_{n+1, m} = R_{n, m} + \Pi_{n, m}^{(R)} \Delta t / M, \\ C_{n+1, m} = C_{n, m} + \Pi_{n, m}^{(C)} \Delta t / M, \\ \Pi_{n+1, m}^{(R)} = \Pi_{n, m}^{(R)} - z_n \Delta t R_{n, m} + \delta_{n, m} + \Delta t F_{n, m}^{(1)}, \\ \Pi_{n+1, m}^{(C)} = \Pi_{n, m}^{(C)} - z_n \Delta t C_{n, m} + \Delta t F_{n, m}^{(2)}, \end{cases}$$

where

$$\begin{cases} F_{n, m}^{(1)} = \Delta t \sum_{j=m}^n \Sigma_{nj} R_{jm}, \\ F_{n, m}^{(2)} = \Delta t \left[\sum_{j=0}^m D_{nj} R_{jm} + \sum_{j=0}^n \Sigma_{nj} C_{jm} \right], \\ \Sigma_{n, m} = -\frac{p\mathcal{J}(n\Delta t)\mathcal{J}(m\Delta t)J^2}{\hbar} \text{Im} \left[C_{n, m} - \frac{i\hbar}{2} R_{n, m} \right]^{p-1} - 4\eta_{n, m} \Theta(t_b - n\Delta t) \Theta(t_b - m\Delta t), \\ D_{n, m} = \frac{p\mathcal{J}(n\Delta t)\mathcal{J}(m\Delta t)J^2}{\hbar} \text{Re} \left[C_{n, m} - \frac{i\hbar}{2} (R_{n, m} + R_{m, n}) \right]^{p-1} + 2\hbar\nu_{n, m} \Theta(t_b - n\Delta t) \Theta(t_b - m\Delta t). \end{cases} \quad (76)$$

The equal time conditions, from Eqs. (33), here assume the simple form

$$C_{n, n} = 0, \quad R_{n, n} = \Pi_{n, n}^{(R)} = \Pi_{n, n}^{(C)} = 0. \quad (77)$$

It is easy to note that Eqs. (76) are causal, implying that we can iteratively compute each minor matrix $C_{0 \leq i \leq n, 0 \leq j \leq n}$ from the knowledge of $C_{0 \leq i \leq n-1, 0 \leq j \leq n-1}$. To understand in detail why, we notice that the row $C_{n, 0 \leq j \leq n-1}$ can

be straightforwardly computed from the minor $C_{0 \leq i \leq n-1, 0 \leq j \leq n-1}$ using Eqs. (76), then the column $C_{0 \leq i \leq n-1, n}$ is immediately obtained from the symmetry relation $C_{n,m} = C_{m,n}$ and the diagonal element $C_{n,n} = 1$ is given by the spherical constraint. The same reasoning holds for the response function, with the only difference that $R_{n,m}$ is not symmetric and $R_{0 \leq i \leq n-1, n} = 0$ due to causality.

We aim to integrate Eqs. (30) and (31) up to some finite time $t_{max} = n_{steps} \Delta t$. With the discretization we chose, the error we make is of order $n_{steps} \Delta t^2$. In order to increase the precision of our results, we improve our method by employing a predictor-corrector algorithm, already used in a similar context in Ref. [69]. In a nutshell, we first predict the $(n+1)$ -th row of the correlation and response function using Eq. (76), and we then correct our result by inserting the result of the prediction in the right-hand sides of the following equations of motion:

$$\begin{cases} \Pi_{n+1,m}^{(R)} = \Pi_{n,m}^{(R)} - \Delta t \frac{z_n R_{n,m} + z_{n+1} R_{n+1,m}}{2} + \delta_{n,m} + \Delta t \frac{F_{n,m}^{(1)} + F_{n+1,m}^{(1)}}{2}, \\ \Pi_{n+1,m}^{(C)} = \Pi_{n,m}^{(C)} - \Delta t \frac{z_n C_{n,m} + z_{n+1} C_{n+1,m}}{2} + \delta_{n,m} + \Delta t \frac{F_{n,m}^{(2)} + F_{n+1,m}^{(2)}}{2}, \\ R_{n+1,m} = R_{n,m} + \Delta t \frac{\Pi_{n,m}^{(R)} + \Pi_{n+1,m}^{(R)}}{2m}, \\ C_{n+1,m} = C_{n,m} + \Delta t \frac{\Pi_{n,m}^{(C)} + \Pi_{n+1,m}^{(C)}}{2m}. \end{cases} \quad (78)$$

For each n -th step, we take a loop over the predictor-corrector scheme \mathcal{N}_L times. In this way, the error we make is of order $n_{steps} \Delta t^{(1+\mathcal{N}_L)}$. For the results presented in the Letter, we have always fixed $\mathcal{N}_L = 2$.

At this point, we observe that Eqs. (78) alone still do not determine the Lagrange multiplier z_n , which is in principle determined by the non-causal equation (equivalent to Eq. (71) of the Letter):

$$z_n = -\frac{\Pi_{n+1,n}^{(C)} - \Pi_{n,n}^{(C)}}{\Delta t} + \Delta t F_{n,m}^{(2)}. \quad (79)$$

As long as the system is coupled to a thermal bath, we solve this issue by making the physical assumption that, due to dissipation, z_n converges at large times to a stationary value, as also observed in Ref. [56]. Due to this asymptotic convergence, we can safely replace the difference $\Pi_{n+1,n}^{(C)} - \Pi_{n,n}^{(C)}$ with the one evaluated at the previous time step, $\Pi_{n,n}^{(C)} - \Pi_{n,n-1}^{(C)}$, in Eq. (79). However, this substitution is not valid for $t > t_b$, where the dynamics is isolated and periodically driven. In the latter scenario, we proceed as discussed in Section and include the discretized version of Eq. (73) in the system of Eqs. (76), so that also z_n can be computed using the predictor-corrector algorithm.

4. Ergodic properties of lattice ϕ^4 model and the p -spin spherical model in absence of a drive

In this section, we discuss the ergodic properties of both the 1D lattice ϕ^4 model and of the p -spin spherical model, in absence of a periodic drive.

We begin by focusing on the ϕ^4 model, whose dynamics is defined by Eq. (19) at $B_0 = 0$. We initialize the system in a Gaussian Gibbs distribution, corresponding to the ϕ^4 Hamiltonian at $\lambda = 0$ and given by

$$\rho_0(\mathbf{x}, \mathbf{p}) = \frac{1}{\mathcal{Z}_0} \exp \left\{ -\frac{\beta}{2} \sum_{k=0}^{N-1} (\tilde{p}_k \tilde{p}_{-k} + \omega_k^2 \tilde{x}_k \tilde{x}_{-k}) \right\} \quad (80)$$

Here, the variables

$$\tilde{x}_k = \frac{1}{\sqrt{N}} \sum_j e^{i \frac{2\pi k}{N} j} x_j, \quad \tilde{p}_k = \frac{1}{\sqrt{N}} \sum_j e^{i \frac{2\pi k}{N} j} p_j, \quad (81)$$

are the Fourier transform of the phase space variables, \mathcal{Z}_0 is a normalization factor and $\omega_k = \sqrt{\omega_0^2 + 2g[1 - \cos(2\pi k/N)]}$ are the normal mode frequencies of the chain. We study the non-equilibrium dynamics evolving from $\rho_0(\mathbf{x}, \mathbf{p})$, realized through a quench in the coupling λ . It is straightforward to show that the initial

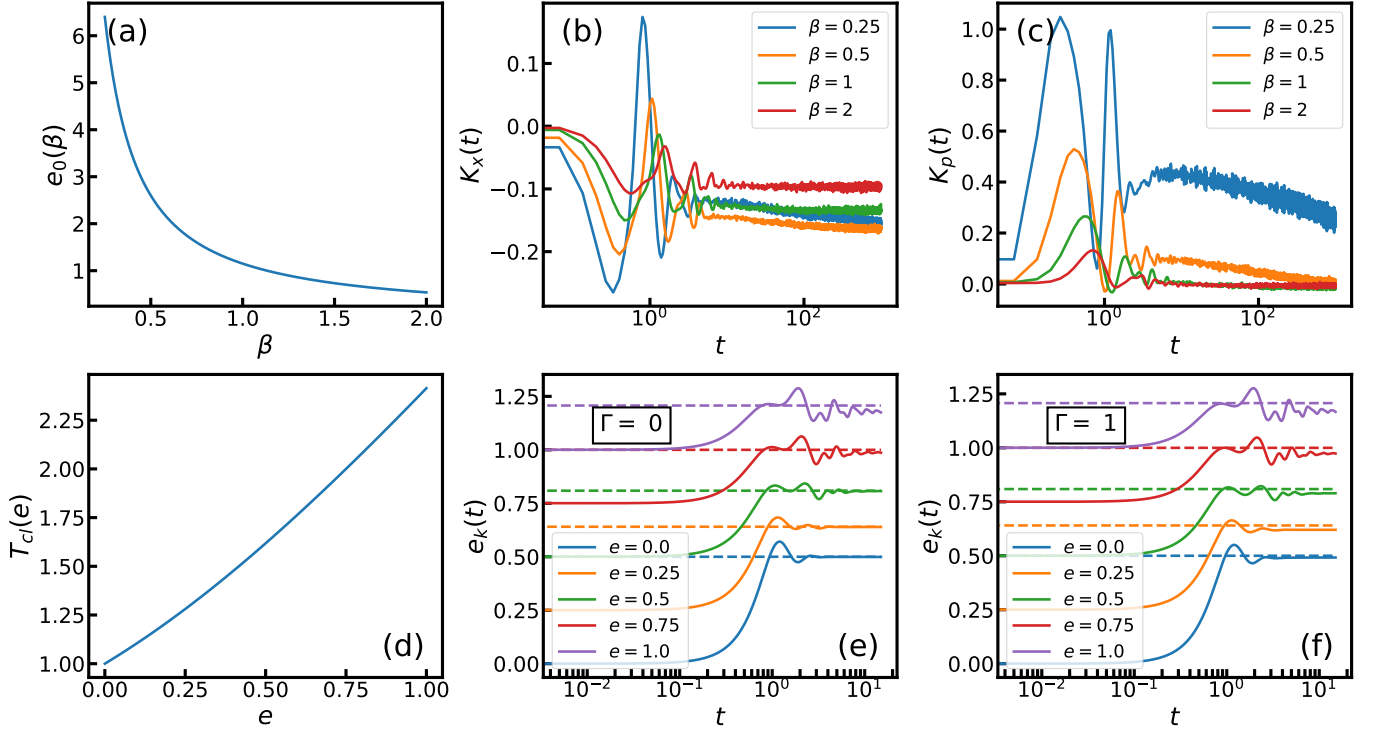


FIG. 4. (Color online). (a-c) Dynamics of the time-independent 1D lattice ϕ^4 model. We fix $N = 100$ and $\omega_0^2 = g = \lambda = 1$. (a) Initial energy density as a function of the inverse temperature, from Eq. (82). (b-c) Kurtosis of the position and momentum degrees of freedom, from Eq. (83). Data are averaged over $\mathcal{N} = 2000$ configurations. (d-f) Dynamics of the time-independent p -spin spherical model. (d) Equilibrium dependence of temperature from the energy density e , from Eq. (84). (e-f) Kinetic energy density from Eq. (85), for the classical ($\Gamma = 0$) and quantum ($\Gamma = 1$) cases. Dashed lines corresponds to the corresponding classical equilibrium expectation values from Eq. (86). We fix $M = J = 1$ and $p = 3$.

energy density of the system is given by

$$e_0(\beta) = \frac{1}{N} \langle H_{\phi^4}(\mathbf{x}, \mathbf{p}) \rangle = \frac{1}{\beta} + \frac{3\lambda}{4\beta^2} \left(\frac{1}{N} \sum_{k=0}^{N-1} \frac{1}{\omega_k^2} \right)^2. \quad (82)$$

The two terms on the right-hand side of Eq. (82) correspond to the averages of the quadratic and the quartic part of the Hamiltonian, respectively. We plot the function $e_0(\beta)$ in Fig. 4-(a), for a range of β roughly corresponding to values of e_0 used in the Letter. We integrate the dynamics for some values of β from the same range and study the time-evolution of the Kurtosis parameters of the phase space degrees of freedom, defined as:

$$K_x(t) = \frac{\langle \sum_i x_i(t)^4 \rangle}{3 \langle \sum_i x_i(t)^2 \rangle} - 1, \quad K_p(t) = \frac{\langle \sum_i p_i(t)^4 \rangle}{3 \langle \sum_i p_i(t)^2 \rangle} - 1. \quad (83)$$

Both $K_x(t)$ and $K_p(t)$ vanish for a Gaussian distribution [66], like the one in Eq. (80), so that $K_x(0) = K_p(0) = 0$. We plot both $K_x(t)$ and $K_p(t)$ in Fig. 4-(b), for several values of β . We observe that $K_x(t)$ and $K_p(t)$ approach an asymptotic value at late times, although the dynamics moderately slows down at low values of β . In particular, $K_p(t)$ asymptotically vanishes, while $K_x(t)$ does not. This result is compatible with the approach to a thermal state of the ϕ^4 model with $\lambda > 0$, which is Gaussian in the momentum variables, but not in the position ones.

Next, we explore the isolated dynamics of the classical and quantum PSM, defined in Eqs. (30) and (31). We fix $B(t) = 0$ and $\mathcal{J}(t) = 1$, to eliminate the periodic drive, and set $t_b = 0$ in Eqs. (69) and (70), to isolate the system from the external bath. We initialize the the Lagrange multiplier $z(t)$, from Eq. (71), to $z(0) = 2e$. This choice corresponds to a non-equilibrium initial state, uncorrelated with the disorder and characterized by a vanishing potential energy and kinetic energy density equal to e [67]. As in the classical case, $\Gamma \equiv \sqrt{\hbar^2/M} = 0$, the equilibrium energy density

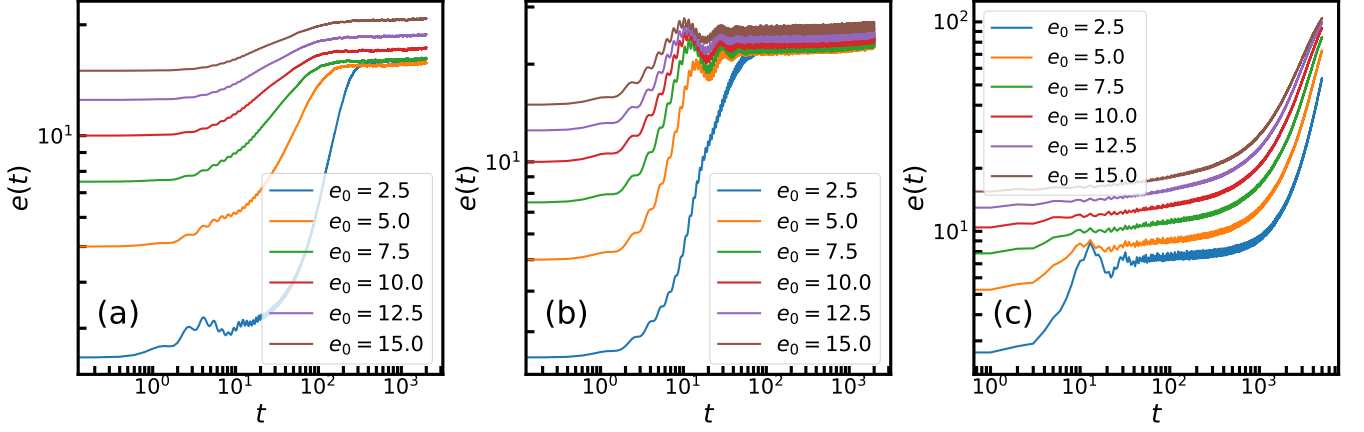


FIG. 5. Average energy density $e(t) = \langle H_{\phi^4}(\mathbf{x}(t), \mathbf{p}(t)) \rangle_0 / N$, for the one dimensional lattice ϕ^4 model, evolving from Eqs. (87). We fix $N = 100$, $\Omega = 2.3$ and $a = \omega_0^2 = g = 1$. The average displayed here is performed over \mathcal{N} configurations, sampled from a microcanonical manifold at various energy density e_0 , for the values of e_0 listed in the legends. We fix $\mathcal{N} = 1000$ and $\lambda = 1$ in panels (a) and (b), while $\mathcal{N} = 500$ and $\lambda = 0.1$ in panel (c). Each panel corresponds to a different form of drive $F_i(\mathbf{x})$. (a) $F_i(\mathbf{x}) = \cos(x_i)$. (b) $F_i(\mathbf{x}) = x_i^2$. (c) $F_i(\mathbf{x}) = x_i$.

e is related to the temperature by [67]

$$T_{cl}(e) = e + \sqrt{e^2 + J^2}, \quad (84)$$

we integrate the dynamics for a set of e roughly corresponding to the initial temperatures T_0 used in the Letter, as it can be inferred from Fig. 4-(d). In Fig. 4-(e), we plot the evolution of the kinetic energy density,

$$e_k(t) = \frac{1}{N} \sum_{i=1}^N \langle \dot{\sigma}_i^2(t) \rangle, \quad (85)$$

for the classical case $\Gamma = 0$. We observe that $e_k(t)$ quickly saturates to a late time plateau, which is compatible with the equilibrium expectation value (dashed lines)

$$e_k^{(mc)} = \frac{e + \sqrt{e^2 + J^2}}{2}. \quad (86)$$

Equation (86) obtained from Eq. (84) and equipartition theorem. This result proves the fast ergodicity of the system, for the range of temperatures considered in the Letter. A similar result is obtained in the quantum case $\Gamma = 1$, as shown in Fig. 4-(f), where the kinetic energy density relaxes roughly to the same plateaus. The similarity between the classical and quantum case suggest that quantum effects are negligible for the parameter we considered.

5. Floquet dynamics with different driving terms

In this section, we investigate the periodically driven dynamics of the classical lattice ϕ^4 model and the p -spin spherical model (PSM). We demonstrate that the energy density profiles highlighted in the Letter remain qualitatively unchanged even when altering the form of the periodic drives.

We begin with the lattice ϕ^4 model, the Hamilton equations of motion of which are given by

$$\ddot{x}_i + \omega_0^2 x_i + \lambda x_i^3 = a \sin(\Omega t) F_i(\mathbf{x}) + g(x_{i+1} - 2x_i + x_{i-1}), \quad (87)$$

where $i = 1 \dots N$. If we set $F_i(\mathbf{x}) = 1$, we recover the same Floquet dynamics examined in the Letter. Instead, here we focus on driving terms corresponding to one of the following possibilities: $F_i(\mathbf{x}) = x_i^2$ or $F_i(\mathbf{x}) = \cos(x_i)$. We numerically integrate Eqs. (87) over an ensemble of \mathcal{N} initial configurations $\{\mathbf{x}(0), \dot{\mathbf{x}}(0)\}$, randomly sampled on the manifold $H_{\phi^4}(\mathbf{x}(0), \dot{\mathbf{x}}(0)) = N e_0$, for several values of e_0 . The resulting average energy density, $e(t) =$

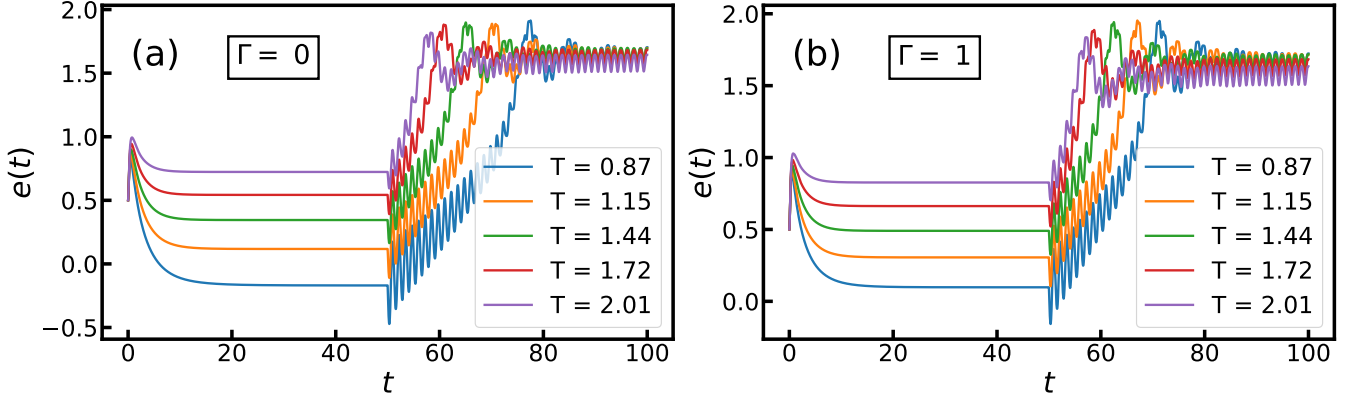


FIG. 6. Average energy density $e(t)$ for the p -spin spherical model, defined in Eq. (34) and evolved using Eq. (30) and Eq. (31). We drive the system by setting $B(t) = 0$ and $\mathcal{J}(t) = 1 + \Delta \sin(\Omega t)$, for $\Delta = 0.5$ and $\Omega = 5$. We also fix $p = 3$, $M = J = 1$, $t_b = 50$. Each panel corresponds to a different value of the dimensionless parameter $\Gamma = \sqrt{\hbar^2/M}$ which quantifies the strength of quantum fluctuations. The different curves in each panel correspond to different initial conditions characterized by their temperature T_0 specified in the keys.

$\langle H_{\phi^4}(\mathbf{x}(t), \dot{\mathbf{x}}(t)) \rangle_0 / N$, is depicted in Fig. 5-(a) and (b). For both driving terms, we consistently observe that $e(t)$ saturates at long times to a finite value e_∞ , underscoring the robustness of the results presented in the Letter across different driving forms. In Fig. 5-(c) we examine a third, more subtle case involving a periodic modulation of ω_0^2 , achieved by setting $F_i(\mathbf{x}) = x_i$. The key observation here is that, for a low initial energy e_0 , the average energy density $e(t)$ exhibits slow but persistent growth within our simulation time scales. This profile, also observed in the closely related $O(N)$ model under the same driving protocol [39], does not provide a definitive indication of either unbounded growth or saturation to a finite value e_∞ . However, we note that the heating diminishes with an increase in the initial energy and eventually disappears for a sufficiently high e_0 . This observation may indicate the existence of an energy threshold at which heating is expected to cease, leading to the saturation of $e(t)$ to a finite value even when evolving from a low initial energy. To validate this conclusion, further investigation is required.

We conduct a similar analysis for the PSM, whose dynamics is governed by the equations of motion (30) and (31). In the Letter, we investigated Floquet dynamics driven by a homogeneous field, achieved by setting $B(t) = B_0 \sin(\Omega t)$ and $\mathcal{J}(t) = 1$ in the Hamiltonian in Eq. (35). Here, our focus shifts to a modulation in the interaction term, achieved by setting $B(t) = 0$ and $\mathcal{J}(t) = 1 + \Delta \sin(\Omega t)$. As illustrated in Fig. 6, the corresponding energy density, Eq. (34), saturates at long times to a finite value, consistently with the results presented in the Letter for a different kind of drive.